Computational analysis and verifications of characteristic modes in real materials

Miers, Zachary; Lau, Buon Kiong

Published in:
IEEE Transactions on Antennas and Propagation

DOI:
10.1109/TAP.2016.2539387

2016

Document Version:
Peer reviewed version (aka post-print)

Computational Analysis and Verifications of Characteristic Modes in Real Materials

Zachary T. Miers, *Member, IEEE,* and Buon Kiong Lau, *Senior Member, IEEE*

***Abstract*—Despite its long history, the Theory of Characteristic Modes has only been utilized in antenna design for perfect electric conductors. This is due to computational problems associated with dielectrics and magnetic materials. In particular, the symmetric form of the PMCHWT surface formulation for the Method of Moments (MoM) solves for both external (real) and internal (non-real) resonances of a structure. The external resonances are the characteristic modes, whereas the internal resonances are not. This article proposes a new post-processing method capable of providing unique and real characteristic modes in all physical mediums, including lossy magnetic and dielectric materials. The method removes the internal resonances of a structure by defining a minimum radiated power, which is found through utilizing the physical bounds of the structure. The characteristic modes found using the proposed method are verified through the use of a MoM volume formulation, time domain antenna simulations, and experiments involving multiple antenna prototypes.**

***Index Terms*—Antenna design, characteristic modes, dielectric resonant antenna, MIMO systems, quality factor**

I. Introduction

SIGNIFICANT insights into the fundamental scattering and radiation properties of any structure can be obtained through analysis of the orthogonal radiation currents it is capable of producing. The Theory of Characteristic Modes (TCM), conceived by Garbacz, Harrington, and Mautz in 1971 [1], [2], solves for these currents in any conducting body. The scattered and radiated modes, or characteristic modes (CMs), of a structure are uniquely solved through an eigenvalue decomposition of the structure's symmetric impedance matrix.

Following its introduction, TCM received interest for analyzing and solving a variety of problems, including radar scattering [1], [3], excitation of large structures with coupling elements (CE) [4], wide-band antenna analysis [5] and antenna shape synthesis [6]. However, TCM remained relatively low profile until recently, when it was recognized in the antenna community as a powerful tool that enables systematic analysis and design of efficient compact antennas [7]-[13]. However, despite substantial existing research on TCM, nearly all prior work focuses on the CMs of perfect electric conductors (PEC). Relatively little attention was given to develop TCM for real materials.

Manuscript received July 29, 2015. This work was supported by Swedish Research Council under Grants No. 2010-468 and No. 2012-4859.

Z. Miers and B. K. Lau are with the Department of Electrical and Information Technology, Lund University, 221 00 Lund, Sweden (e-mail: Zachary.Miers @eit.lth.se; Buon_Kiong.Lau@eit.lth.se).

In [14], Harrington et al. first proposed a method to solve for CMs in real materials, which is based on the eigenvalue decomposition of the structure's impedance matrix for a Method of Moments (MoM) volume integral equation (VIE) formulation. However, computation of a volume impedance matrix was, and still is, computationally prohibitive. Hence, Chang and Harrington developed a computationally efficient surface integral equation (SIE) formulation in [15]. However, [14] and [15] focus on constructing the mathematical proof behind solving for the CMs of any object; no computed CMs are shown.

The proof given in [15] was first used in [16] to extract the impedance matrix of a PEC object in close proximity to a dielectric object. This work did not analyze, compute, or utilize the modes within the dielectrics, but only studied the CMs of the PEC object. The first known computation of CMs of a dielectric object was published in [17]. The paper stated that the CMs from the VIE formulation in [14] satisfy field orthogonality and every CM radiates unity power, thus fulfilling the requirements for TCM. Furthermore, it briefly computed and examined the CMs of a simple lossless object, which were obtained using the SIE formulation outlined in [15]. It was stated that the CMs solved using [15] did not satisfy field orthogonality, nor did every CM radiate unity power. The modes which radiated unity power were labelled physical modes whereas all other modes were labeled non-physical modes. No details were provided on how these computations were carried out and why an eigenvalue decomposition using the MoM SIE formulation gives rise to CMs which do not radiate unity far-field power. Furthermore, no analysis or results were provided on real materials which must dissipate some amount of power, and thus theoretically cannot not radiate unity far-field power.

This article proposes a new and practical post-processing method that yields the correct CMs in real materials. Herein, the Poggio-Miller-Chan-Harrington-Wu-Tsai (PMCHWT) SIE formulation for MoM [18] will be analyzed, and shown that when forced into symmetry, the CM solution is susceptible to the MoM internal resonance problem [18]. These internal resonances do not correspond to real structural resonances, and can be found in the simplest of structures which utilize this formulation. A power threshold defined from the structure's physical bounds can be used to isolate the CMs corresponding to internal resonances. To demonstrate the effectiveness of the proposed method, the CMs of homogeneous dielectric and magnetic composite cubes found with this method are compared to those found using the VIE

formulation. Two characteristic modes of the structures are then excited using coupling feeds, and these real CMs are verified using far-field simulations and measurements. In this context, the main contributions of this work are:

- Explaining the appearance of non-real modes when the CMs of a structure are computed by means of the PMCHWT SIE MoM formulation.
- Providing an effective method for isolating and removing the non-real CMs of an object that are found using a MoM SIE formulation.
- Verifying the computed CMs to be real CMs through multiple means: VIE formulation, full wave time domain analysis, and measured physical prototypes.

The paper is organized as follows: Section II presents an overview of the SIE MoM formulations and explains the MoM internal resonance problem. A novel method to identify and remove non-real CMs attributed to internal resonances is described in Section III. Section IV overviews a VIE MoM formulation and how it is applied to a specific structure. Section V solves for the CMs in several lossless, lossy, and magnetically doped composite dielectric cubes, and compares these modes to the VIE CMs. In Section VI, the far-fields of selected SIE and VIE CMs are compared against the CMs excited in antenna simulations and physical antenna prototypes. Finally, the main findings and conclusions are provided in Section VII.

II. Internal Resonance Problem

Previous publications which rely on CM analysis to aid in the understanding and design of antenna structures have utilized the PEC formulation of CMs [2]. As can be seen from existing literature (e.g., [3]-[13]), the PEC formulation can solve a large variety of different antenna related problems. However, PEC and perfect magnetic conducting (PMC) objects are some of the simplest scattering objects [18]. Structures built entirely from these classes of materials are often referred to as impenetrable, as the tangential field is zero across the surface of the object, i.e., no power can penetrate the object. However, many antenna-related problems involve materials which are both penetrable (dielectric objects and magnetic objects) and lossy. In these types of objects it is possible for power to flow both into and through the object. When MoM integral equations are used to solve for the electromagnetic properties of all materials, there are two formulations which can be utilized to set up the required systems of equations. The first and most often applied is the surface integral equation (SIE), whereas the volume integral equation (VIE) is less often applied due to its high computational complexity. The SIE formulation is often used when the problem consists of homogeneous materials, whereas the VIE formulation is preferred when the problem consists of extremely heterogeneous materials [18].

There are three main types of SIE formulations: electric field integral equation (EFIE), magnetic field integral equation (MFIE), and combined field integral equation (CFIE). The standard EFIE and MFIE suffer from what is known as the internal resonance problem. The existence of these internal resonances can be easily understood in some cases (PEC and PMC objects), whereas it is less understood in other cases (dielectric and magnetic objects) [18]. For a closed PEC object, the internal resonances can be related to the non-radiating resonance cavity mode; however, this is not as easily explained for dielectric objects, as the resonance frequency of a dielectric scatterer must be complex due to radiation dampening (i.e., energy cannot be perfectly confined within the object) [18]. However, the internal resonances of an object can be proved through different Gedanken experiments [19]; for brevity this will not be reviewed but interested readers should refer to [19] for more information.

These internal resonances can be eliminated through proper combination of the EFIE, MFIE, electric combined integral equation (ECIE), and magnetic combined integral equation (MCIE). This is possible because whereas all the individual equations suffer from internal resonances, the mathematics causing the resonances are different among them [20]. These equations provide four equations and two unknowns. In order to reduce the equation space so that there are the same number of equations as unknowns, the number of equations should be reduced to two. This is done through a linear combination of four integral equations as shown in (1) and (2), where a_i, b_i, c_i, and d_i are the coupling coefficients within the domain D_i. For SIE problems there are two domains (i.e., i = 1, 2), these domains correspond to the penetrable, homogeneous, isotropic scatterer (D_2) and homogeneous, isotropic background (D_1) [20]. It should be noted that the specific values of the coupling coefficients, within the domain, have a significant effect on properties of the final SIE solution [21].

$$\textit{Combined Equation 1: } a_i\,ECIE + b_i\,EFIE \tag{1}$$

$$\textit{Combined Equation 2: } c_i\,MCIE + d_i\,MFIE \tag{2}$$

There are several ways of combining these equations to obtain a unique solution free from internal resonances. A computationally efficient way is to use a linear combination which forces two of the integral equations to zero; this can be done by setting $a_i = c_i = 0$ or $b_i = d_i = 0$. The two most used SIE formulations utilize this method and are referred to as the NMüller and PMCHWT MoM SIE formulations [18]. The NMüller formulation, the most popular variant of the Müller formulation, sets $a_i = \mu_i$ and $c_i = \varepsilon_i$, where μ_i is the absolute permeability and ε_i is the absolute permittivity within the domain D_i. The PMCHWT formulation is the most widely implemented SIE solution and uses $b_i = d_i = 1$. Both the PMCHWT and NMüller formulations have been shown to effectively create a lossy boundary condition such that all null-space solutions (internal resonances) can only occur at complex frequencies [18]. A proof in [22] showed that any choice of a_i, c_i or b_i, d_i for which $a_i c_i^*$ or $b_i d_i^*$ (where $(\cdot)^*$ is the complex conjugate) is equal to a real and positive number will provide a unique solution (free from internal resonances) to an SIE formulation.

Formulations which hold true to this proof are capable of providing an impedance matrix for any 3D structure. This impedance matrix can then be used to solve for the

characteristic modes of the structure if and only if the impedance matrix $[Z]$ is symmetric (i.e., $\langle [B],[Z][C]\rangle = \langle [Z][B],[C]\rangle$, where $\langle\cdot,\cdot\rangle$ is the inner product operator and $[B],[C]$ are arbitrary square matrices) [2]. Neither the NMüller formulation nor the PMCHWT formulation provides a symmetric impedance matrix. It is not clear how to force NMüller into symmetry, but it is possible to force PMCHWT into symmetry, as was shown in [15]. The remainder of this manuscript will utilize the PMCHWT method which sets $b_i = d_i = 1$. The matrix construction of the PMCHWT formulation is shown in (3).

$$\underbrace{\begin{bmatrix} [Z_{mn}^{+}+Z_{mn}^{-}] & [-\beta_{mn}^{+}-\beta_{mn}^{-}] \\ [\beta_{mn}^{+}+\beta_{mn}^{-}] & [Y_{mn}^{+}+Y_{mn}^{-}] \end{bmatrix}}_{[\tilde{Z}]} \begin{bmatrix} J \\ M \end{bmatrix} = \begin{bmatrix} E \\ H \end{bmatrix} \tag{3}$$

While $[\tilde{Z}]$ in (3) is not symmetric, each individual submatrix within $[\tilde{Z}]$ is independently symmetric and defined by

$$Z_{mn}^{\pm} = j\omega L_{mn}^{\pm} + \frac{1}{j\omega} S_{mn}^{\pm}\,, \tag{4}$$

$$Y_{mn}^{\pm} = \frac{Z_{mn}^{\pm}}{\left(\eta^{\pm}\right)^2} \tag{5}$$

$$\beta_{mn}^{\pm} = \iint_s \Lambda_m(r)\cdot\left(\Lambda_n(r')\times\nabla G^{\pm}(r,r')\right) ds \tag{6}$$

where

$$L_{mn}^{\pm} = \mu^{\pm}\left\langle \Lambda_m; G^{\pm}; \Lambda_n \right\rangle, \tag{7}$$

$$S_{mn}^{\pm} = \frac{1}{\varepsilon^{\pm}}\left\langle \nabla\cdot\Lambda_m, G^{\pm}, \nabla\cdot\Lambda_n \right\rangle, \tag{8}$$

$$G^{\pm}(r,r') = \frac{e^{jk^{\pm}(r-r')}}{4\pi(r-r')}. \tag{9}$$

In these equations $k^{\pm}$, $\eta^{\pm}$, $\mu^{\pm}$, $\varepsilon^{\pm}$ are the wavenumbers, intrinsic impedances, permeability, and permittivity of the internal (-) and external (+) media, Λ_n is the associated MoM basis function, and $\langle\cdot,\cdot,\cdot\rangle$ is the intersection of all subspaces. The impedance matrix of this combined equation can be forced into symmetry through the addition of a complex scalar to (2), creating the new symmetric impedance operator and a modified version of the PMCHWT formulation as described by [15]

$$\begin{bmatrix} [Z_{mn}^{+}+Z_{mn}^{-}] & -j[-\beta_{mn}^{+}-\beta_{mn}^{-}] \\ j[\beta_{mn}^{+}+\beta_{mn}^{-}] & [Y_{mn}^{+}+Y_{mn}^{-}] \end{bmatrix} \begin{bmatrix} J \\ jM \end{bmatrix} = \begin{bmatrix} E \\ jH \end{bmatrix}, \tag{10}$$

where the symmetric impedance matrix (Z) of (10) is now

$$Z = \begin{bmatrix} [Z_{mn}^{+}+Z_{mn}^{-}] & -j[-\beta_{mn}^{+}-\beta_{mn}^{-}] \\ j[\beta_{mn}^{+}+\beta_{mn}^{-}] & [Y_{mn}^{+}+Y_{mn}^{-}] \end{bmatrix}. \tag{11}$$

This symmetric formulation was introduced by Harrington in [15] prior to the proof in [22]. Reference [22] revealed that any choice of $b_i\, d_i^*$ must be real and positive to provide a unique solution to an SIE formulation. Therefore, the symmetric form of the combined equation (10) no longer fulfills this condition for a unique solution. The choice of coupling coefficients in (11) allows the matrix to be symmetric, but moves the complex frequency null-space solutions into the real solution space, i.e., the internal resonances are moved into the solution space.

Hence, the internal resonances within the impedance matrix are individually solved for, and placed within the TCM solution space as individual CMs. Many publications have shown that all TCM methods solve for the internal resonances of a structure [2], [23]. However, with a properly formed impedance matrix these internal resonances are easily disregarded as their eigenvalues, in the solution space, are approximately infinity. This is due to the resonant frequency of the null space solutions being located outside of the real frequency domain. However, this is no longer valid when the impedance matrix holds the form of the symmetric PMCHWT matrix shown in (10). The eigenvalue solution set for the impedance matrix in (11) solves for the structure's internal resonances which now occur at real frequencies. In theory these internal resonant modes can be easily removed as the associated surface currents are non-radiating and as such the modes cannot be normalized using the method described by (16) in [2]. However, in practice the structures domain is built using approximate expansion functions, e.g. Rao-Wilton-Glisson (RWG) edge elements. As a result the associated surface currents radiate a power greater than zero [18]. The non-zero radiated power allows for the characteristic currents to be normalized. These internal resonances create a serious challenge for solving many MoM problems. As a direct result of this internal resonance problem there has been no obvious solution to allow for TCM to be effectively applied to an SIE MoM formulation. However, a unique TCM identity can be exploited to provide a solution to this problem, as will be shown in Section III.

III. Identification of TCM Internal Resonances

TCM is unique when compared to other MoM equations as it provides an independent solution to each orthogonal current mode a structure is capable of supporting (internal and external). This is possible as the CMs are derived through an orthogonal decomposition of the real and imaginary parts of the symmetric impedance matrix. Proper formulation of a weighted eigenvalue equation leads to the solution for these orthogonal currents, herein referred to as characteristic currents. This specific weighted eigenvalue equation is formulated as

$$[X](J_n) = \lambda_n [R](J_n)\,, \tag{12}$$

where $[R]$ and $[X]$ are the real and imaginary parts of the symmetric impedance matrix $[Z]$, and J_n is the n^{th} CM associated with the n^{th} eigenvalue λ_n. When this equation is solved using the impedance matrix in (11) it is not obvious how to distinguish between eigenvalues associated with internal resonances and those associated with external resonances. For loss-free structures, both the characteristic currents and characteristic far-fields are fully orthogonal [14].

This is true for the characteristic currents, but no longer true for the characteristic far-fields due to the radiated far-field pattern of the internal resonances [2] [14].

It can be argued that these internal resonances can be removed by calculating the far-field radiated power of a structure using

$$P = \frac{1}{2}\oiint_{S_\infty} E_n \times H_n^* ds\,, \tag{13}$$

where E_n and H_n are the electric and magnetic fields associated with the eigenmode J_n,, and S_∞ is the sphere at infinity. In principle this is true as the far-field radiated power of the internal resonances should be equal to zero. However, due to the utilization of approximate expansion functions and application of eigenmode current normalization, the radiated power of internal resonances can be greater than zero. It should be noted that due to small number rounding errors powers greater than unity can be found in some structures after applying eigenmode current normalization. Furthermore, when losses are included in (11) through the introduction of complex permeability and permittivity, some external (real) resonances will radiate less power than some of the normalized internal resonances.

One simple and intuitive solution is to remove these internal resonances through MoM mesh perturbation, thus changing the individual basis functions. When the MoM mesh is changed, the expansion functions must also change. This will relate to a change in the amount of far-field power radiated by internal resonant modes. If the same mode under two different mesh perturbations radiate different amounts of far-field, the mode can be associated with an internal resonance. However, initial studies revealed that in practice it is not always possible to understand how much the mesh should be perturbed to guarantee every internal resonant mode radiates a significant enough power difference to be detected and identified as an internal resonance. Therefore, the mesh perturbation approach is not studied further in this paper.

To resolve the aforementioned problems, a new equation can be introduced to solve for which modes are associated with internal and external resonances. This can be done by computing the quality factor (Q) associated with each mode. The quality factor is a measure of how much energy is stored versus dissipated in a structure. If it is possible to determine the Q for each mode, the maximum amount of energy lost can be calculated. This allows for computation of the radiation efficiency of an antenna [24], [25]. When applied to antenna modes as calculated by TCM, modes with a radiation efficiency (derived from Q) not equal to the radiated power efficiency as calculated by (13), can be associated to an internal resonance. The efficiency of an antenna can be equated to the antenna quality factors, where the quality factor is calculated by (14) and the total efficiency (15) [26], [27], [28]. In (14) and (15), $(\cdot)_{tot}$, $(\cdot)_{rad}$, $(\cdot)_{sw}$, $(\cdot)_d$, and $(\cdot)_c$, are, respectively, the quality factors and radiated power associated with the total structure, radiation, surface wave, dielectric, and conductor. In electrically compact structures the surface wave is difficult to excite, and does not support any significant bandwidth (i.e. $Q_{sw} \approx \infty$). For these reasons this article assumes in order to simplify the overall computation while maintaining accurate results. However, it should be noted that the exact value of Q can be calculated from the difference between the internal and external electric and magnetic fields.

$$\frac{1}{Q_{tot}} = \frac{1}{Q_{rad}} + \frac{1}{Q_{sw}} + \frac{1}{Q_d} + \frac{1}{Q_c} \tag{14}$$

$$\eta_{tot} = \frac{P_{rad}}{P_{rad} + P_c + P_d + P_{sw}} \tag{15}$$

It was shown in [25] that these equations can be used to calculate the total losses an antenna is capable of supporting at a given Q. A simplified form of (15) that lower bounds the total efficiency of an antenna is shown in Eq. (16),

$$\eta_{rad} \geq \frac{Q_{com}}{Q_{com} + Q_{rad}}\,, \tag{16}$$

$$\frac{1}{Q_d} = \tan\delta_d + \tan\delta_m = \frac{\varepsilon''}{\varepsilon'} + \frac{\mu''}{\mu'}\,, \tag{17}$$

where η_{rad} is the radiated power efficiency of the antenna, $Q_{com} = Q_{sw} + Q_d + Q_c$ is the sum of the quality factors of each component as calculated by (14) [24]-[26], and Q_{rad} is the quality factor of the antenna as calculated by TCM. It may be of interest to the reader that the quality factor can be related back to the complex permeability ($\varepsilon = \varepsilon' - j\varepsilon''$) and permeability ($\mu = \mu' - j\mu''$) of a material by means of the dielectric and magnetic loss tangents (17). Q_{rad} was defined in [29] and [30], and can be found using the symmetric PMCHWT characteristic currents [31] using

$$Q_{rad} = \frac{\omega[I_n]^H[X'][I_n] + \left|[I_n]^H[X][I_n]\right|}{2[I_n]^H[R][I_n]}\,, \tag{18}$$

where $[I_n]$ is the eigencurrent of the nth mode, $[R]$ and $[X]$ are the real and imaginary parts of the impedance matrix $[Z]$, $[X'] = [\partial X/\partial\omega]$, $[\bullet]^H$ is the conjugate transpose operator, and $I_n = [J_n \quad jM_n]^T$. J_n and M_n are purely real electric currents and purely imaginary magnetic currents, respectively. Using these definitions, it can be shown that the real part of the inner product $\langle [I_n]^*, [Z][I_n] \rangle$ is identical to the mode's radiated power found by means of the Poynting Theorem. However, the imaginary part of $\langle [I]^*, [Z][I] \rangle$, which is defined as λ_n, is not equal to the corresponding imaginary part of the Poynting Theorem, i.e., $2\omega(W_m - W_e)$, relating to the difference in the stored magnetic energy W_m and electric energy W_e. However, the calculation of Q in (18) is based on the characteristic currents I_n and the impedance matrix $[Z]$, and hence unaffected by λ_n. For EFIE PEC problems (i.e., $I_n = [J_n]$), λ_n corresponds to the imaginary part of the Poynting Theorem [32].

Using (16) and the associated quality factors in (18), it is possible to determine if a mode is related to an internal or external resonance. The modes which do not adhere to (16) are modes associated with internal resonances whereas all other modes are external resonances. This method, henceforth called

physical bounds method, can be applied to the CMs computed using (12) and the symmetric SIE MoM impedance matrix (11). The final computed external resonances can be easily verified by means of properly solving for the VIE CMs and matching the VIE modes to this SIE formulation. However, as will be described in Section IV, this can be difficult as solving for the VIE CMs is not trivial.

IV. CM Solution to a MoM VIE Formulation

It has been shown that an eigenvalue decomposition of the MoM impedance matrix obtained using a VIE formulation provides only the external CMs for any real material [14]. However, this method has not been applied in the literature due to its extremely high computational complexity. Computing CMs using the VIE formulation is computationally prohibitive due to the large number of basis functions, i.e., proportional to the square of the number required for a well-conditioned SIE formulation [18]. When using the prohibitively large VIE impedance matrix to solve for the CMs of an object, the total solution time increases relative to the cube of the computational time required for calculating the CMs of an object using a SIE formulation [33]. This increase in time is due to the computations required to solve for the impedance matrix which requires matrix inversion operations to properly decompose the impedance matrix into individual characteristic modes and currents.

Applying volume-based TCM to anything other than electrically very small objects is not currently practical for engineering applications. However, in theory it is possible to exploit a VIE method to provide the external CMs of any object. These modes can then be used to prove that non-real CMs are associated with a direct SIE decomposition of both (3) and (11), and applying (16) to (11) solves for non-real CMs. Although this does not prove if a TCM method will always solve for non-real CMs, it does show if a TCM method solves for any non-real CM at a defined frequency for a defined structure. Therefore, this process allows for the identification of non-real modes in a given solution space that were formed by a specific SIE TCM method.

Whereas the majority of existing MoM VIE formulations apply the same physics, slight differences can be found in them, as was seen in the different ways to apply (1) and (2) in Section II. The VIE analysis presented in this article applies the matrix formulation as defined by (4.46)-(4.48) in [18]. These equations provide an impedance matrix which can be decomposed into CMs using (63) in [14]. Using this matrix formulation, the number of basis functions can be reduced by half when applied to objects consisting of either only electric or magnetic materials. In this specific case the resulting impedance matrix is symmetric and the CMs can be found using (12). However, when utilizing these equations on an object consisting of both electric and magnetic materials the solution space must be forced into symmetry [14].

The accuracy of the mentioned VIE solution depends significantly on the quality of the volume mesh used to quantify the object. The solution accuracy degrades when the mesh quality is not sufficient. This type of inaccuracy is derived from large basis elements as the edge element tetrahedral expansion functions give rise to surface singularities on the surface of each tetrahedron. Surface singularities result in elements of the impedance matrix overestimating the amount of stored energy within any given tetrahedral [18]. This is important to remember when a VIE method is used to solve for the CMs of an object. If an object's volume mesh tetrahedral are too large, CM with high quality factors can result in an overestimation of the amount of stored energy in a tetrahedral thus resulting in the eigenvalues being different than reality.

The effect of eigenvalue inaccuracies derived from poor VIE mesh qualities can be seen when solving for the CMs of a single object over a variety of different mesh densities. In this article the SIE CMs of dielectric cubes measuring 2.54cm × 2.54cm × 2.54cm are compared against the VIE solution in Section V. The small differences between the VIE solution and the SIE solution can be observed in modes with high Q; these differences are due to the quality of the VIE mesh. The effect of mesh density on a dielectric cube is shown in Fig. 1. This figure uses three different mesh densities to solve for the CMs of a loss-free dielectric cube (relative permittivity ε_r = 9.4). The three different mesh densities shown consist of 928, 1640, and 6256 basis elements. As the number of mesh elements increase the values converge to an SIE solution point at a nearly exponential rate (observed). This convergence can be seen in the figure, where each solution converges to a point equal to one of the CM values found by an SIE solution. It should be noted that while a VIE solution requires an extremely dense tetrahedral mesh to converge there are also known convergence problems associated with solving the SIE impedance matrix when using RWG basis elements. While the SIE RWG convergence rate can be increased in many different ways, for the purposes of this study the number of RWG mesh elements (created in the open source GMSH code) was iteratively increased until the SIE impedance matrix produced eigenvalues (between $-20 < \lambda < 20$) which changed by no more than 10^{-2}. This condition is generally reached when the SIE mesh element length was approximately equal to $1/20^{th}$ of the effective wavelength of the structure being characterized.

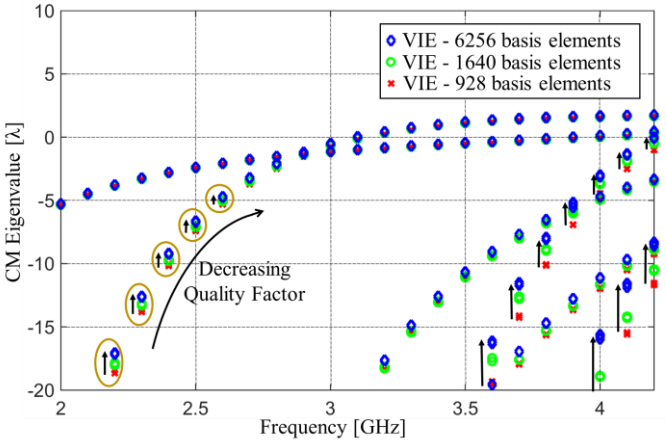

Fig. 1. Impact of mesh quality on the accuracy of CM eigenvalues for a dielectric cube.

The CMs for a mesh density consisting of 6256 basis elements is still considered to be a coarse VIE mesh. However, this tetrahedral density is computationally prohibitive for CM solutions, as the VIE simulation containing 6256 bases elements took 373,242 seconds to complete. Both the VIE and SIE solutions in the article were computed using Matlab codes using the built-in eigensolver. All solutions throughout this article were completed on an Intel Core i7-5960 PC with 32 GB of DDR4 memory and no parallel processing. In the following section, it will be seen that the physical bounds method provides an SIE solution that is as accurate as this VIE solution and is significantly more computationally practical.

V. Comparison of SIE Modes to VIE Modes

For conciseness, this article will not explore all facets of the physical bounds method presented in Section III. However, in an effort to illustrate the differences between methods, five different dielectric resonators were chosen and analyzed to show the differences between the two SIE solutions and the VIE solution. It should be noted that the internal resonance problem is not only found in purely dielectric problems, but in any problem which utilizes the symmetric form of the PMCHWT SIE formulation to solve for the MoM impedance matrix. The impedance matrices for the SIE solutions in this manuscript were found using an in-house, Matlab-based, PMCHWT MoM solver and verified using the computationally efficient commercial MoM solver, FEKO. On the other hand, all VIE impedance matrices were found using FEKO. The impedance matrices were then exported to Matlab for CM processing. Beyond the computation of the impedance matrices, all computations were carried out using in-house Matlab codes. Each dielectric resonator was designed to be identical in size whereas the material properties of each resonator were varied. Each dielectric resonator measures 2.54cm × 2.54cm × 2.54cm and is made from a composite consisting of a base material of alumina (Al_2O_3). Different losses were added to the alumina through carbon loading, while magnetic permeability was added through doping the alumina with $BaFe_{12}O_9$ (0.15 micron). The simulated material parameters were extracted from physical prototypes [34], and the approximate properties of each cube are shown in Table I, where μ_r denotes relative permeability.

TABLE I
Properties of Dielectric and Magnetic Cube Resonators

Cube	ε_r	tan δ_d	μ_r	tan δ_m
NL	9.4	0	1.0	0
L0	9.4	0.003	1.0	0
L1	9.3	0.012	1.0	0
L5	9.1	0.053	1.0	0
M3	8.7	0.026	2.6	0.034

Each cube is labeled to simplify recurring references to the specific material properties of the individual cube structures. The cubes are labeled as follows:

- Cube NL is loss-free. It is made of a non-real material and is only used for simulation purposes.
- Cube L0 is made of real Al_2O_3 yielding a permittivity loss tangent (tan δ_d) of 0.003.
- Cube L1 adds pure carbon powder, obtaining a loss tangent of 0.012.
- Cube L5 adds pure carbon powder, obtaining a loss tangent of 0.053.
- Cube M3 is doped with $BaFe_{12}O_9$ (obtained from Sigma-Aldrich Incorporated) to add some permeability and magnetic losses to the cube (μ_r = 2.6, tan δ_m = 0.034) while achieving ε_r = 8.7 and moderate tan δ_d = 0.026.

Each of these cubes has different CMs across frequency. The first resonance of the loss-free cube structure (cube NL) is located near 3.0 GHz. To show the differences between CM simulation methods and material types, the structures' CMs were analyzed from 2.0 GHz to 4.2GHz. Each of the methods presented produces a set of eigenvalues for each structure at each frequency point. However, for completeness, while reducing extraneous information from this article, the CMs produced using (3) and (11) will only be plotted for the ideal loss-free cube (Cube NL).

The CMs, as calculated through the decomposition of (3), do not satisfy any of the CM requirements. Some of the requirements which are not satisfied by the resulting CMs are the non-orthogonal characteristic far-fields and characteristic currents. Additionally, by definition electrically small structures support a low number of excitable or near-resonant CMs (with -1.5 < λ < 1.5). As can be seen from Fig. 2, the decomposition of (3) produces more than 12 near-resonant CMs at 2GHz, and as many as 25 at 4GHz. These results are expected as the impedance matrix of (3) is not symmetric, which is contrary to the requirement in TCM computations.

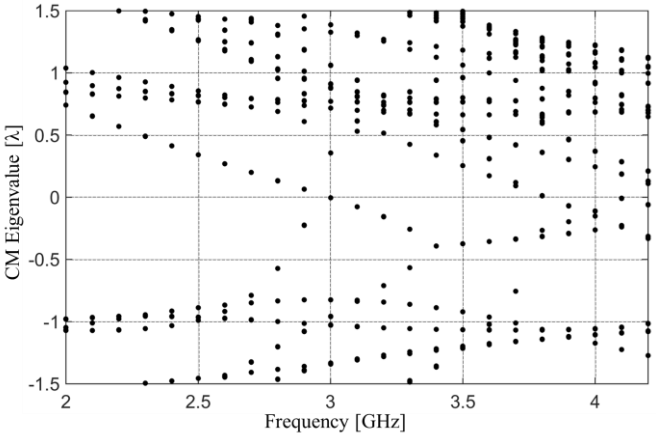

Fig. 2. First 25 CMs of the non-symmetric PMCHWT impedance matrix which are near resonance. In particular, 12 modes are near resonance at 2GHz, where the structure is electrically too small to support any near resonant modes at this frequency.

The symmetric form of the PMCHWT MoM impedance matrix (11) provides the CMs corresponding to both internal and external resonances of the structure, as was described in Section II. Figure 3 shows the CMs of both the VIE solution

as well as the modes of (11) for Cube NL. The modes shown with positive eigenvalues for this specific structure are related to internal resonances. These internal resonant modes are not present in the VIE solution; and whereas the currents are orthogonal, the far-field patterns are not orthogonal. It should be noted that the computational time of this SIE solution took 226 seconds while the computational time of the VIE solution took 373,242 seconds (4.32 days). If the VIE modes in Fig. 2 are compared to the modes in Fig. 3 it is apparent that an eigen decomposition of (11) does not provide a correct or usable TCM solution.

It is possible to remove these internal resonances from the problem space using one of two methods: the power thresholding method that was expressed as a preliminary observation in [17], or the proposed physical bounds method that was described in Section III. The power thresholding method was applied using a trial and error procedure within this manuscript. This was done by iteratively decreasing the radiated power threshold until all VIE modes between $-20 < \lambda_n < 20$ were present in the solution, or until a significant number of non-real modes were observed within these bounds. It should be noted that this procedure is optimistic, as it requires the VIE solution to be known for each of the simulations prior to applying the power thresholding method, which is impractical.

Figure 4 shows the CMs for SIE thresholding, SIE physical bounds, and the VIE method. It can be seen that all three methods work well for the non-realistic material which has no losses. Small discrepancies between the SIE formulations and the VIE formulation in modes with high Q can be attributed to the coarse VIE meshing, as discussed in Section IV. The computational times for the power thresholding and physical bound methods are greater than the direct decomposition of (11) which is seen in Fig. 3. This is because the radiated power must be computed for each CM. The computational time for power thresholding was 302 seconds whereas the computational time of the defined physical bounds was 518 seconds. The time difference between these SIE methods is due to the required quality factor computation. To compute the quality factor, an additional closely spaced frequency step was added 50 kHz from the plotted simulation point. This allows for a valid computation of the Q of each mode using (18).

With the help of VIE CMs in the trial-and-error procedure, SIE power thresholding has been found to be as accurate as, and faster than, both the physical bounds and VIE solutions, when applying TCM to loss-free dielectric materials. However, when small amounts of loss are added into the simulation, power thresholding does not always provide an accurate and reliable solution, even when assisted by known CMs from VIE. When very small losses are added to any object, the power thresholding technique provides reliable results only near resonance. For example, non-real CMs can be found at eigenvalues greater than $|\lambda_n| = 10^5$ for Cube L0, which has a small dielectric loss tangent of 0.003. When designing antennas using TCM, eigenvalues with this order of magnitude are not relevant. However, from a purely theoretical perspective, the solution is not completely accurate.

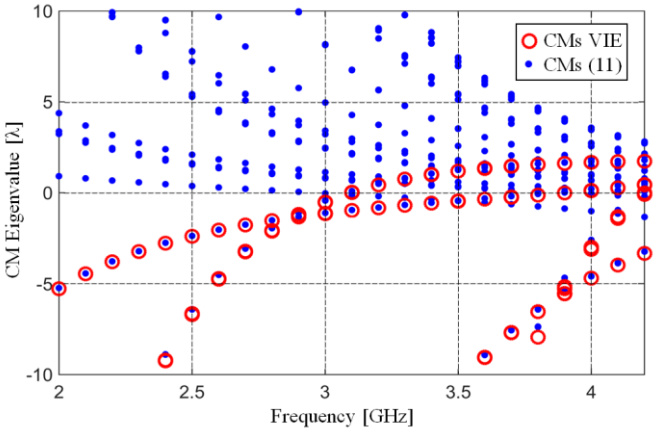

Fig. 3. Comparison of CMs of the symmetric PMCHWT SIE impedance matrix (11) and the CMs of the VIE formulation for Cube L0. The symmetric SIE impedance matrix produces several inductive modes near resonance, these are non-real modes as this structure does not support inductive eigenmodes at frequencies below 3GHz.

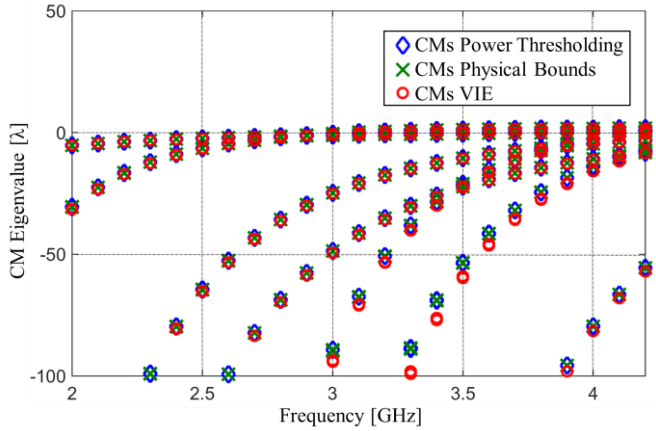

Fig. 4. Comparison and visualization of the all the SIE and VIE CM solutions between $-100 < \lambda < 50$ for the loss free cube (Cube NL).

When realistic losses are added to an object (e.g., Cube L1), the power thresholding method becomes unreliable, whereas the physical bounds method remains stable. The CMs of Cube L1 are shown in Fig. 5. The unreliability of the power thresholding method is due to the presence of non-real CMs which pass through resonance. These non-real modes are detrimental to TCM antenna design, as these "resonant modes" are likely to be chosen as candidates for antenna designs, but in reality cannot be excited and will not radiate power. This problem of non-real CMs worsens as the loss of the structure increases. Figure 6 shows the modes of Cube L5, and it can be seen that several non-real CMs exist in the power thresholding solution, whereas the physical bounds solution remains accurate.

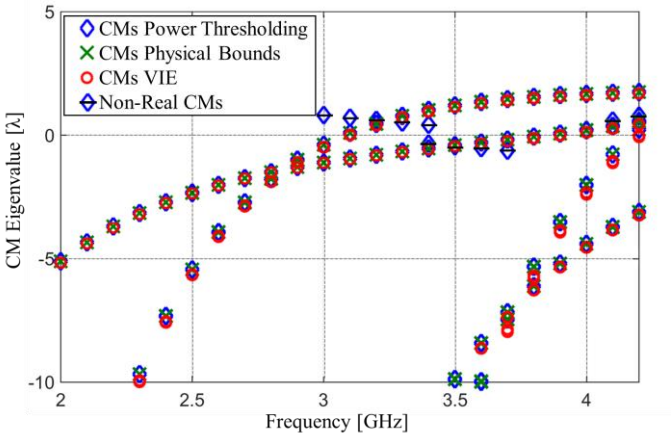

Fig. 5. Comparison of the first four characteristic modes for the SIE and VIE solutions of Cube L1. Non-real CMs are only found in the power thresholding method. The non-real modes found by this method are shown with a black line through the blue diamond marker to indicate the non-real CMs found in this specific solution.

Materials with mixed permittivity and permeability present a problem to all TCM solution sets. Even though magnetic materials may not be as common as dielectric materials in antenna design, they can play a vital role in antenna miniaturization [35] and absorbing materials [36]. In recent years, nano-ferrites have been proven useful at higher frequencies, with reduced loss while maintaining high permeability [37] These new materials, while still lossy, can significantly reduce the resonant frequency of multi-GHz dielectric resonator antennas (DRAs). For these reasons, it is important to understand the limitations of TCM design using materials with mixed permittivity and permeability.

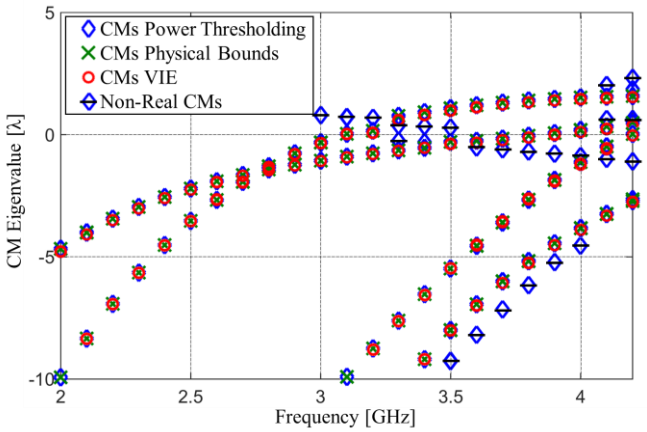

Fig. 6. Comparison of the first four characteristic modes for the SIE and VIE solutions of Cube L5. Non-real modes are only found in the power thresholding solution and are indicated by a black line through a blue diamond marker.

When materials of mixed composition are used to calculate the CMs of a VIE solution, the number of basis functions used is doubled. This is problematic as the computational time increases with the number of basis functions (see section IV). When evaluating the CMs of Cube M3 using the same number of meshing elements, the computational time becomes unrealistic. To determine the VIE CM solution for Cube M3, the number of mesh elements was reduced by half, corresponding to half as many basis functions. This causes significant computational error in high Q modes. However, the VIE CM solution will provide only real CM modes, thus non-real CMs and missing CMs can be found within the SIE solution set. The VIE CMs for Cube M3 are shown as red circles in Fig. 7. Point A in this figure shows an example of the error which is observed in high Q modes.

The power thresholding solution in Fig. 7 consists of both missing and non-real CMs. As described previously, the radiated power threshold was increased until all modes were observed or until a significant number of non-real CMs appeared. Point B in Fig. 7 indicates a few of the power thresholding modes that cannot be linked to any mode in the VIE solution set, therefore these modes are determined to be non-real CMs. Apart from the existence of a significant number of non-real modes, many real CMs are missing in the solution. At points A and C, modes matching the VIE solution can only be found within the physical bounds solution, whereas the power thresholding solution has no matching CMs in these areas.

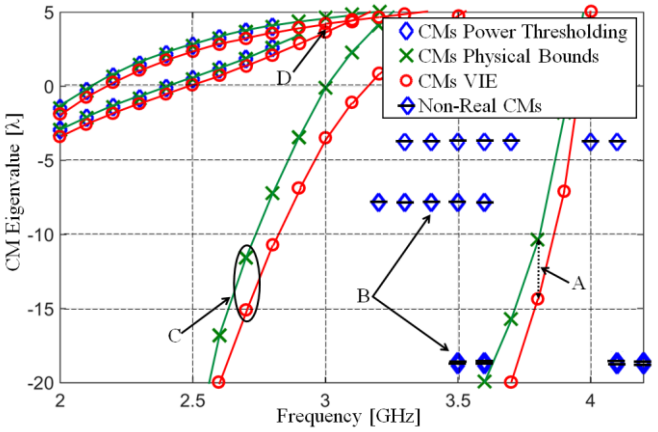

Fig. 7. Comparison of notable and interesting characteristic modes for the SIE and VIE solutions of Cube M3. Far-field CM tracking [34] was utilized to link modes at different frequencies (solid lines added) to help identify the corresponding modes for the different solutions. Non-real modes are only found in the power thresholding solution and are indicated by a black line through a blue diamond marker.

The problems associated with using the power thresholding method to compute the CMs of dielectric/magnetic objects are highlighted in Figs. 5-7, and the speed of current computers places severe limitations on computing CMs using a VIE MoM impedance matrix. However, one problem is observed in the physical bounds method that may place some limitations on this method. At point D in Fig. 7, one of the VIE modes is missing from the physical bounds solution. Application of the physical bounds method requires that two impedance matrices be computed at adjacent frequencies (in this case 50kHz) in order to compute the Q of the given mode. In order to calculate the correct Q, the modes must not be degenerated, i.e. it should be possible to properly track the same mode at two adjacent frequency points; this is where a problem arises.

Degenerated modes cause problems in determining the

correct currents at frequency points where two modes cross. When (12) is applied to an impedance matrix the associated eigenvalues are not sorted between one frequency point and the next, and locations of CM crossover cannot be located [38], thus degenerated modes cannot be determined. If a degenerated mode occurs for a specific mode, the currents can be effected, thus altering the Q of the mode. Advanced CM tracking techniques have been developed in recent years, these advances allow the physical bounds method to perform as well as it does. However, because internal resonances have correlated far-fields, the tracking method in [38] cannot be utilized, thus a current based tracking solutions must be applied. In [38], it was shown that tracking techniques which use characteristic currents often fail in many ways, including when differences between modes are limited to high currents in small regions of the structure. The mode at point D may be degenerated, and cannot be detected using current based tracking methods [39]. The degenerated mode changes currents and the quality factor, thus one modal point was determined to be an internal resonance rather than properly defined as a real CM. Future improvements in current based tracking solutions, or proper removal of degenerated modes, should solve this problem. However, the high accuracy of the presented physical bounds method allows for TCM to be used to effectively design antennas in any material.

VI. Verification of CM Analysis

The CMs found using the physical bounds method can be utilized to design antennas and understand how to adapt antennas for specific performance goals. The CMs found in Section V for each cube can be used to design antenna feeds, or coupling elements (CEs), which will primarily only excite specific CMs. To verify that a given CM is successfully excited, the radiated far-field pattern of the physical structure can be analyzed to determine the CMs which are excited within the structure [23]. If the primary excited mode corresponds to that of the intended CM (from Section V), then this CM is verified to be a physical structural resonance (i.e., a real mode). Whereas the theoretical proof of these modes being real was given in [15] for SIE structures and [14] for VIE structures, here a physical representation of these proofs is shown.

The near-fields of the first two resonances of each cube structure were evaluated for the placement of CEs. The first CM of Cube L0, L1, and L5 maintained a resonant frequency of approximately 3.1GHz (see Table II), whereas the second CM for these cubes maintained a resonant frequency of approximately 4.0GHz. The modal resonance for both modes slightly increased in frequency as the loss of the structure increased. The first two CM resonances of Cube M3 were significantly below that of the other cubes, i.e., the first resonance was seen at 2.1GHz and the second resonance at 2.4GHz. Once the real CMs of the structure are found, the corresponding characteristic near-fields and currents of each CM can be used to determine the placement of current or near-field CEs. When properly designed and implemented these CE will only couple energy into the selected CM, and thus the antenna will radiate that specific mode. This design procedure is different than that of traditional DRA coupling elements, which often utilize either a slot-coupled aperture or a vertical monopole. These types of DRA CE designs require a ground plane and dielectric cutouts which may influence the specific CMs previously found. However, it may be of interest to the reader that the CM near fields can be used in the same manner as those of natural modes (i.e., TE/TM modes) when using CMs for DRA specific designs.

The CEs for each resonance were designed using cross sectional cuts of electric and magnetic near-fields for the real characteristic modes 1 and 2. The near-field cross sectional cuts of Cube L1 are shown in Fig. 8. The near-fields of mode 1 show that the mode primarily radiates electric near-fields in region A (Fig. 8). This indicates that if z-directed electric-field energy can be coupled into the cube structure in this region, mode 1 of the structure should be effectively excited. It is well known that a small non-resonant dipole stores a significant amount of electric-field energy along the long axis of the dipole in its reactive near-field region. If the small dipole is placed along the dotted line in region A of Fig. 8, the dipole will couple electric-field energy into the cube structure and effectively excite mode 1. The near-fields of mode 2 are significantly different than those of mode 1 and show that the mode primarily radiates magnetic near-fields around the structure as seen in region B (Fig. 8). This indicates that if a CE is introduced which can induce the same fields in that region, the near-fields will couple energy into mode 2, and mode 2 will be excited. A small non-resonant loop stores magnetic-field energy along the length of the loop structure in its reactive near-field region. Therefore, when a small loop is placed around the structure in the x-y plane (dotted line along region B in Fig. 8) the loop will couple magnetic-field energy into the cube structure and effectively excite mode 2. The final design parameters and dimensions of the electric CE are shown in Fig. 9(a), while the dimension of the magnetic CEs are shown in Fig. 9(b).

The two distinctive CEs which should correspond to two orthogonal antennas were analyzed using the Finite-difference time-domain (FDTD) solver in CST, and simulated from 1GHz to 4.5GHz. The simulated resonant frequencies of each cube are shown in Table II. This table provides the CM resonance frequencies, the frequencies at which each cube antenna's imaginary impedance crosses zero, and where the antenna's real impedance is equal to 50Ω. It should be noted that $\lambda_n = 0$ is not related to the ideal 50Ω matching frequency (i.e., Im(Z) = 0Ω and Re(Z) = 50Ω), but rather it indicates where $W_m = W_e$ for these structures. When designing antenna structures using CMs, the optimal 50Ω antenna match must often be realized through the use of matching components. The fed cube structures (Fig. 9) have a resonance frequency for Im(Z) = 0Ω within 80 MHz of where λ_n crosses zero. The antenna feeds did not utilize a matching circuit in an effort to preserve the imaginary impedance's characteristics. This implies that the CE are properly exciting the expected characteristic current. As expected, the CM resonance frequency is unrelated to the ideal 50Ω match frequency.

Thus, when comparing λ_n = 0 to Re(Z) = 50Ω a constant frequency offset is not observed.

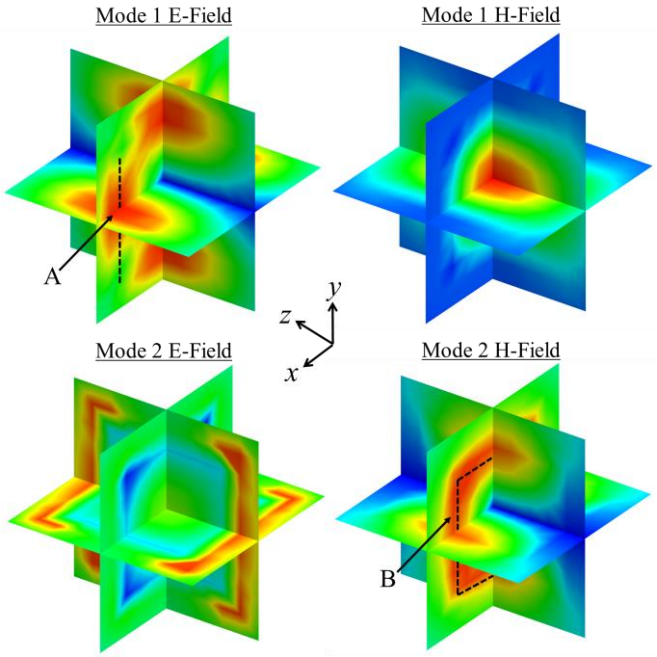

Fig. 8. *xy*, *xz*, and *yz* cross sectional cuts of the electric and magnetic near-fields (magnitudes only) for modes 1 and 2 of Cube L1. The dashed line in region A corresponds to a predicted location to place an electric coupling element which will couple electric energy into mode 1, whereas the dashed line in region B corresponds to a predicted location of a magnetic coupling element which will feed couple magnetic energy into mode 2.

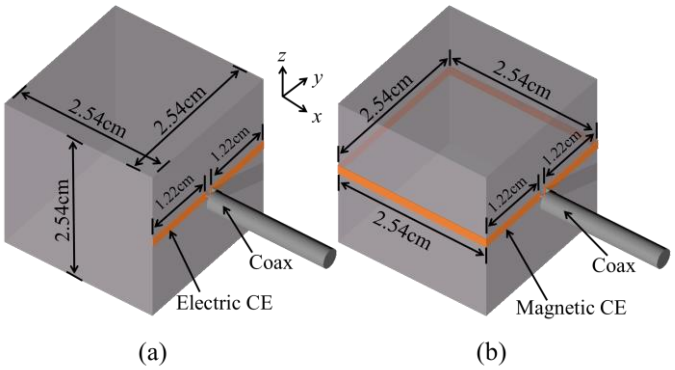

Fig. 9. (a) The electric CE and (b) the magnetic CE were designed using the CM cross-sectional near-fields. The loaded resonance frequency of both CE structures are not resonant near the characteristic modal resonance frequency.

TABLE II
MODAL RESONANCE AND SIMULATED ANTENNA RESONANT FREQUENCY

Cube Type	Feed Type	Modal Resonance	Simulated Im(Z) = 0	Simulated Re(Z) = 50Ω
Cube NL	Electric	3.08 GHz	3.11 GHz	3.24 GHz
Cube L0	Electric	3.08 GHz	3.10 GHz	3.24 GHz
Cube L1	Electric	3.10 GHz	3.13 GHz	3.24 GHz
Cube L5	Electric	3.18 GHz	3.22 GHz	3.24 GHz
Cube M3	Electric	2.12 GHz	2.10 GHz	2.21 GHz
Cube NL	Magnetic	4.03 GHz	4.10 GHz	4.14 GHz
Cube L0	Magnetic	4.05 GHz	4.11 GHz	4.14 GHz
Cube L1	Magnetic	4.05 GHz	4.11 GHz	4.15 GHz
Cube L5	Magnetic	4.09 GHz	4.17 GHz	4.17 GHz
Cube M3	Magnetic	2.41 GHz	2.47 GHz	2.49 GHz

The modal far-field energy contribution to the individual simulated far-field patterns can be determined using the modal reconstruction theory presented in [23]. As can be observed from Fig. 10, the predicted mode contributes more than 90% of the energy of each simulated antenna's far-field pattern. Mode 4 contributes 7.2% of the far-field energy of Cube L5's simulated antenna resonance. This was determined to be due to the length of the magnetic CE used to excite the structure. This contribution can be reduced by reducing the overall length of the magnetic CE. If the CE's length is reduced by means of placing the CE 3mm within the cube's surface, the contribution of mode 4 to the antenna pattern is reduced to 0.8%. However, placing the CE within the cubes surface is not easily implemented in a real structure; therefore, the choice was made to place the CE on the exterior of the cubes surface. Less than 1% of the total far-field energy was contributed to the simulated antenna patterns by non-existent modes (i.e., modes from the feed structure itself, which is not part of the original cube structure), higher order modes, or the individual coupling elements.

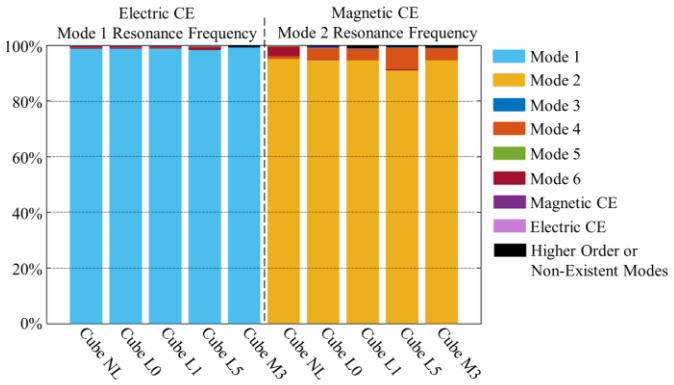

Fig. 10. The simulated antenna far-field patterns have a significant modal contribution from the expected modes for all ten structures. Each modal reconstruction was computed for the simulated frequency where Im(Z) = 0, as shown in Table II.

The described CEs were implemented on the physical cube structures (i.e., Cube L0-L5 and Cube M3 in Section V), and fed using a standard 50Ω coaxial cable (see Fig. 11). The measured resonant frequencies of each cube is shown in Table III. The simulated (Table II) and measured (Table III) resonant frequencies correspond extremely well to one another. It should be noted that resonant frequencies in Table III utilized a balun as well as absorbing material around the coaxial cable. A high correlation between the simulated and measured resonances is expected as the simulated material properties were defined by the physical properties of each prototype. The small differences between the measured and simulated resonance frequencies were determined to be due to cable coupling effects (significant), variation in CEs (marginal), and simulation mesh density (minimal).

TABLE III
MODAL RESONANCE AND MEASURED ANTENNA RESONANT FREQUENCY

Cube Type	Feed Type	Modal Resonance	Measured Im(Z) = 0	Measured Re(Z) = 50Ω
Cube L0	Electric	3.08 GHz	3.10 GHz	3.30 GHz
Cube L1	Electric	3.10 GHz	3.21 GHz	3.39 GHz
Cube L5	Electric	3.18 GHz	3.15 GHz	3.18 GHz
Cube M3	Electric	2.12 GHz	2.22 GHz	2.44 GHz
Cube L0	Magnetic	4.05 GHz	3.92 GHz	3.98 GHz
Cube L1	Magnetic	4.05 GHz	3.94 GHz	4.06 GHz
Cube L5	Magnetic	4.09 GHz	4.21 GHz	4.29 GHz
Cube M3	Magnetic	2.41 GHz	2.52 GHz	2.66 GHz

Each physical structure's 3D complex radiation pattern was measured in an anechoic chamber at Lund University. As with the simulated radiation patterns, the modal reconstruction theory in [23] was applied to determine the individual modal contribution of the final measured antenna far-field patterns. During this measurement campaign, it was determined that the feed cable radiated a significant amount of far-field energy. The coaxial cable effects were determined to be the cause of the radiation discrepancies. These discrepancies were discovered through evaluating the far-field envelope correlation coefficient (ECC) of the simulated and measured antennas. The ECC was found to be as low as 0.6 in some prototypes. When a 5cm feed cable was introduced into the simulation, the ECC increased by as much as 0.2, thus demonstrating the significant effect the coaxial cable has on the final radiated pattern.

When mapping the modal contribution of the cubes without compensating for the cable effects, more than 40% of the radiated energy could not be mapped to any mode (non-existent modes). To reduce the effect of the feed cable, a balun was connected to the feed point of each cube, and magnetic radar absorbing material covered the first 5cm of the cable directly following the balun. The same setup was used to obtain the results in Table III. The modal contributions (Fig. 12) show that the expected mode contributes more than 80% of the energy of the measured far-field antenna patterns. The small discrepancies between the measured and simulated prototypes are believed to be due to remaining feed cable effects as well as practical problems associated with measuring physical prototypes at these frequencies. The normalized 2D principal plane cuts for the simulated and measured patterns for Cube L0 are shown in Fig. 12 (mode 1) and Fig. 13 (mode 2). Note, these figures utilize linear scaling to more effectively show the differences between the simulated and measured patterns.

Figures 9 and 11 as well as Tables II and III clearly show strong agreement between the physical bounds CMs and VIE CMs computed in Section V. The physical antenna resonances can be strongly linked to the CMs of the structure by means of modal reconstruction. This provides evidence that the first two modes solved for in Section V correspond to a real resonances. These resonances can be effectively, and realistically, excited to radiate far-field energy. Therefore, this provides evidence that the first two resonant modes of these structures cannot be attributed to a MoM internal resonance, and thus, must be attributed to real CMs.

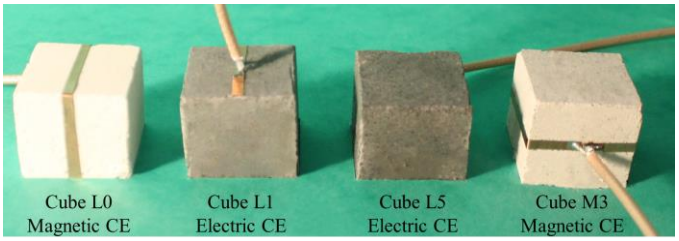

Fig. 11. Four of the eight physical prototypes that were fabricated. Two of the structures show how the electric CE was implemented, while the other two structures show how the magnetic CE was implemented.

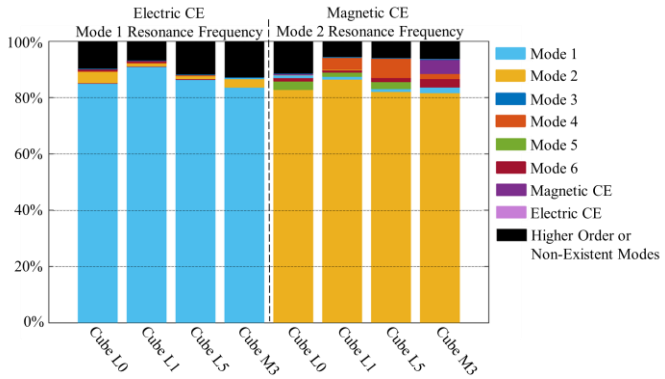

Fig. 12. The measured antenna far-field patterns have a high (>80%) modal contribution from the expected modes for the eight physical structures. Each modal reconstruction was computed for the measured frequency where Im(*Z*) = 0 as shown in Table III.

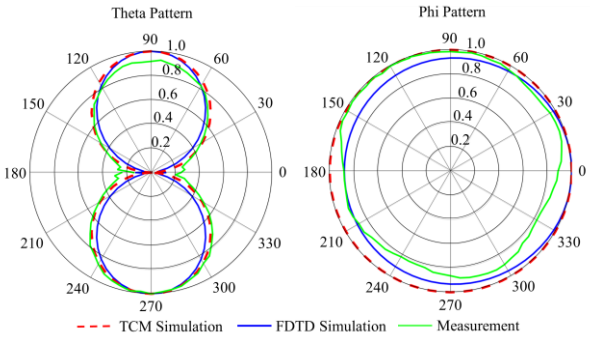

Fig. 13. Normalized simulated and measured patterns of Cube L0 for mode 1 (Electrical CE) at 3.10 GHz. The Theta and Phi patterns are aligned with the coordinate system shown in Fig. 8 and Fig. 9.

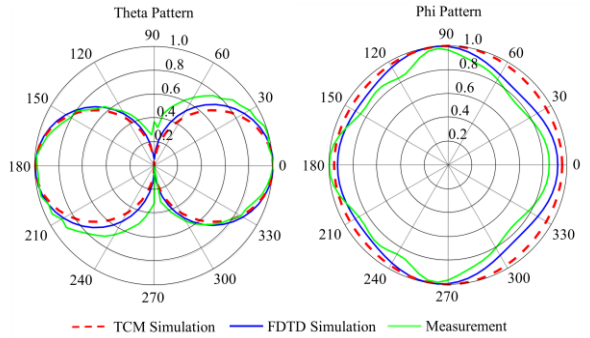

Fig. 14. Normalized simulated and measured patterns of Cube L0 for mode 2 (Magnetic CE) at 3.92 GHz. The Theta and Phi patterns are aligned with the coordinate system shown in Fig. 8 and Fig. 9.

VII. Conclusions

In this work, a new and practical physical bounds post-processing method for obtaining the real CMs of any impedance matrix found using a MoM surface formulation was developed, presented, and verified. This new method provides the real CMs of any material by utilizing the inherent properties of TCM to locate and remove internal resonances formed by an improperly formulated CFIE SIE MoM equation. This work demonstrated the viability of this method using a symmetric form of the PMCHWT SIE formulation for MoM. The symmetric PMCHWT impedance matrix was analyzed and it was shown that any CM solution found using this impedance matrix is susceptible to the MoM internal resonance problem, including but not limited to: dielectric resonators, printed circuit board (PCB) substrates, and antenna support structures. Utilizing the fundamental properties of TCM, it is possible to isolate the CMs that correspond to internal resonances through either basis function perturbation, power thresholding [17], or the proposed physical bounds defined threshold.

Power thresholding and the proposed method of isolating the CMs that correspond to real resonances were analyzed against each other, as well as against a VIE formulation. The physical bounds method gave superior results when compared against the power thresholding method. The power thresholding method provided inaccurate results in lossy materials, and no specific defined threshold could be found to be acceptable for all low loss material types and shapes. However, the physical bounds method was found to provide an efficient and correct result when compared directly against the VIE CMs of several cube structures of different material properties. Degenerated modes may cause problems when using the physical bounds method; if modes are degenerated across frequency, real modes can be defined as internal modes and internal modes can be defined as real modes. The high accuracy of current algorithms allowed this method to perform extremely well, but future improvements in removing degenerated modes will lead to even higher accuracy in a physical bounds solution set.

The CMs of several cube-shaped dielectric structures were used to develop eight different physical antennas. The far-field patterns of the excited DRAs were used to map the theoretical CMs to the physical resonances of the structure. The mode mapping verified that the CMs were related to real resonances. Time domain simulations of these cube structures also confirm the accuracy of the achieved experimental results.

This work shows that it is now possible to obtain CMs in lossy real materials in a computationally efficient manner, allowing the TCMs to be used for engineering applications. When properly applied, this proposed method of calculating the theoretical CMs of a structure can be used to better understand the underlying properties of any antenna, as well as to design and construct antennas for specific performance goals.

Acknowledgment

The authors would like to thank FEKO for donating their commercial EM software, Mats Gustafsson for his insights regarding stored energy and method of moments, and the anonymous reviewers for their valuable comments which improved the quality of this work.

References

[1] R. J. Garbacz and R. Turpin, "A generalized expansion for radiated and scattered fields," *IEEE Trans. Antennas Propag.*, vol. 19, no. 3, pp. 348-358, May 1971.

[2] R. F. Harrington and J. R. Mautz, "Theory of characteristic modes for conducting bodies," *IEEE Trans. Antennas Propag.*, vol. 19, no. 5, pp. 622-628, Sep. 1971.

[3] J. R. Mautz, and R. F. Harrington, "Modal analysis of loaded N-port scatterers," *IEEE Trans. Antennas Propag.*, vol. 21, no. 2, pp. 188-199, Mar. 1973.

[4] E. H. Newman, "Small antenna location synthesis using characteristic modes," *IEEE Trans. Antennas Propag.*, vol. 27, no. 4, pp. 530-531, Jul. 1979.

[5] M. Hilbert, M. A. Tilston, and K. G. Balmain, "Resonance phenomena of log-periodic antennas: characteristic-mode analysis," *IEEE Trans. Antennas Propag.*, vol. 37, no. 10, pp. 1224-1234, Oct. 1989.

[6] D. Liu, R. J. Garbacz, and D. M. Pozar, "Antenna synthesis and optimization using generalized characteristic modes," *IEEE Trans. Antennas Propag.*, vol. 38, no. 6, pp. 862-868, Jun. 1990.

[7] K. K. Kishor and S. V. Hum, "A pattern reconfigurable chassis-mode MIMO antenna," *IEEE Trans. Antennas Propag.*, vol. 62, no. 6, pp. 3290-3298, Jun. 2014.

[8] J. J. Adams and J. T. Bernhard, "A modal approach to tuning and bandwidth enhancement of an electrically small antenna," *IEEE Trans. Antennas Propag.*, vol. 59, no. 4, pp. 1085-1092, Apr. 2011.

[9] Z. Miers, H. Li, and B. K. Lau, "Design of bandwidth-enhanced and multiband MIMO antennas using characteristic modes," *IEEE Antennas Wireless Propag. Lett.*, vol. 12, pp. 1696-1699, 2013.

[10] J. J. Adams and J. T. Bernhard, "Broadband equivalent circuit models for antenna impedances and fields using characteristic modes," *IEEE Trans. Antennas Propag.*, vol. 61, no. 8, pp. 3985-3994, Aug. 2013.

[11] D. Manteuffel and R. Martens, "A concept for MIMO antennas on small terminals based on characteristic modes," in *Proc. Int. Workshop Antenna Tech. (IWAT'2011)*, Hong Kong, P. R. China, Mar. 7-9, 2011, pp. 17-20.

[12] E. Safin and D. Manteuffel, "Manipulation of characteristic wave modes by impedance loading," *IEEE Trans. Antennas Propag.*, vol. 63, no. 4, pp. 1756-1764, Apr. 2015.

[13] R. Rezaiesarlak and M. Manteghi, "Design of chipless RFID tags based on characteristic mode theory (CMT)," *IEEE Trans. Antennas Propag.*, vol. 63, no. 2, pp. 711-718, Feb. 2015.

[14] R. F. Harrington, J. R. Mautz, and Y. Chang, "Characteristic modes for dielectric and magnetic bodies," *IEEE Trans. Antennas Propag.*, vol. 20, no. 2, pp. 194-198, Mar. 1972.

[15] Y. Chang and R. F. Harrington, "A surface formulation for characteristic modes of material bodies," *IEEE Trans. Antennas Propag.*, vol. 25, no. 6, pp. 789-795, Nov. 1977.

[16] R. T. Maximidis, C. L. Zekios, T. N. Kaifas, E. E. Vafiadis, and G. A. Kyriacou, "Characteristic mode analysis of composite metal-dielectric structure, based on surface integral equation/moment method," in *Proc. 8th Eur. Conf. Antennas Propag. (EuCAP'2014)*, The Hague, The Netherlands, Apr. 6-11, 2014, pp. 2822-2826.

[17] H. Alroughani, J. L. T. Ethier, and D. A. McNamara, "Observations on computational outcomes for the characteristic modes of dielectric objects," in *Proc. Int. Symp. Antennas Propag.*, Memphis, TN, USA, Jul. 6-11, 2014, pp. 844-845.

[18] W. C. Chew, M. S. Tong, and B. Hu, "Integral equations for electromagnetic and elastic waves," in *Lectures on Computational Electromagnetics #12*, 1st ed. San Rafael, CA., USA: Morgan Claypool, 2009, ch. 3-4, pp. 43–102.

[19] W. C. Chew and J. M. Song, "Gedanken experiments to understand the internal resonance problems of electromagnetic scattering," *Electromagn.*, vol. 27, no. 8, pp. 457–472, 2007.

[20] P. Ylä-Oijala, M. Taskinen, and S. Järvenpää, "Surface integral equation formulations for solving electromagnetic scattering problems with iterative methods," *Radio Sci.*, vol. 40, 2005.
[21] P. Ylä-Oijala, J. Markkanen, S. Jarvenpaa, and S. Kiminki, "Surface and volume integral equation methods for time-harmonic solutions of Maxwell's Equations," *J. Prog. Electromagnetics Res. (PIER)*, vol. 149, pp. 15–44, 2014.
[22] J. R. Mautz and R. F. Harrington, "Electromagnetic scattering from a homogeneous body of revolution," Tech. Rep. TR-77-10, Dep. Electrical and Computer Eng., Syracuse University, Nov. 1977. Available: http://www.dtic.mil/dtic/tr/fulltext/u2/a086508.pdf
[23] E. Safin and D. Manteuffel, "Reconstruction of the characteristic modes on an antenna based on the radiated far field," *IEEE Trans. Antennas Propag.*, vol. 61, no. 6, pp. 2964-2971, Jun. 2013.
[24] A. Arbabi and S. Safavi-Naeini, "Maximum gain of a lossy antenna," *IEEE Trans. Antennas Propag.*, vol. 60, no. 1, pp. 2-7, Jan. 2012.
[25] J. Rahola, "Effect of antenna *Q* to the radiation efficiency of tunable antennas," in *Proc. 8th Eur. Conf. Antennas Propag. (EuCAP'2014)*, The Hague, The Netherlands, Apr. 6-11, 2014, pp. 3285-3288.
[26] R. F. Harrington, "Effect of antenna size on gain, bandwidth, and efficiency," *Journal of Research Nat. Bur. Stand. D. Radio Propag.*, vol. 64D, no. 1, Jan.-Feb., 1960.
[27] A. N. Willson, Jr. and H. J. Orchard, "Insights into digital filters made as the sum of two allpass functions," *IEEE Trans. Circuits Syst. I: Fund. Theory Appl.*, vol. 42, no. 3, pp. 129-137, Mar. 1995.
[28] H. F. Lee and W. Chen, "General formulation of the cavity model," in *Advances in Microstrip and Printed Antennas*, 1st ed. Covent Garden, London, Imperial College Press, 2011, ch. 3, pp. 39–55.
[29] R. F. Harrington and J. R. Mautz, "Control of radar scattering by reactive loading," *IEEE Trans. Antennas Propag.*, vol. 20, no. 4, pp. 446-454, Jul. 1972.
[30] M. Gustafsson, D. Tayli, and M. Cismasu, "Q factors for antennas in dispersive media," Lund University, Department of Electrical and Information Technology, P.O. Box 118, S-221 00 Lund, Sweden, Tech. Rep. LUTEDX/(TEAT-7232)/1–24/(2014), 2014, http://www.eit.lth.se. [Online]. Available: http://lup.lub.lu.se/record/4648444
[31] T. K. Wu and L. L. Tsai, "Scattering from arbitrarily shaped lossy dielectric bodies of revolution," Radio Sci., vol. 12, no. 5, pp. 709–718, 1977
[32] Y. Chen and C. Wang, *Characteristics Modes Theory and Applications in Antenna Engineering*. Hoboken, New Jersey: Wiley, 2015, pp. 48-49.
[33] R. B. Lehoucq, D. C. Sorensen, and C. Yang, *ARPACK Users Guide: Solution of Large-Scale Eigenvalue Problems with Implicitly Restarted Arnoldi Methods*, SIAM, Philadelphia, 1998.
[34] J. Mosig, J. C. Besson, M. Gex-Farby, and F. Gardiol, "Reflection of an open-ended coaxial line and applications to nondestructive measurement of materials," *IEEE Trans. Instrum. Meas.*, vol. 30, pp. 46-51, Mar. 1981.
[35] L. Jaejin, H. Yang-Ki, L. Woncheol, G. S. Abo, P. Jihoon, S. Won-Mo, and B. Seok, "Role of small permeability in gigahertz ferrite antenna performance," *IEEE Magnetics Lett.*, vol. 4, pp. 5000104, 2013.
[36] H. H. B. Rocha, F. N. A. Freire, R. C. S. Costa, R. S. T. Sohn, G. Orjubin, C. Junqueira, T. Cordaro, and A. S. B. Sombra, "Dielectric resonator antenna: Operation of the magnetodielectric composites Cr0.75Fe1.25O3 (CRFO)/Fe0.5Cu0.75Ti0.75O3 (FCTO)," *Microw. Opt. Tech. Lett.*, vol. 49, no. 2, pp. 409-413, Dec. 2006.
[37] N. N. Al-Moayed, M. N. Afsar, U. A. Khan, S. McCooey, and M. Obol, "Nano ferrites microwave complex permeability and permittivity measurements by T/R technique in waveguide," *IEEE Trans. Magnetics*, vol. 44, no. 7, pp. 1768-1772, Jul. 2008.
[38] Z. Miers and B. K. Lau, "Wide band characteristic mode tracking utilizing far-field patterns," *IEEE Antennas Propag. Lett.*, vol.14, no., pp.1658-1661, Aug. 2015
[39] D. J. Ludick, J. V. Tonder, and U. Jakobus, "A hybrid tracking algorithm for characteristic mode analysis," in *Proc. Int. Conf. Electromagnetics in Advanced Appl. (ICEAA'2014)*, Palm Beach, FL, Aug. 3-8, 2014, pp. 455-458.

Zachary T Miers (S'07-M'10) was born in Boulder, CO and received his B.Sc. and M.Sc. from the University of Colorado at Boulder, USA. While at the University of Colorado he was awarded a National Science Foundation scholarship for Mentoring through Critical Transition Points, as well as an image processing research grant from University of Colorado Applied Mathematics department. After graduating he has held multiple career positions in RF and microwave technologies, working to develop antennas for both commercial and government applications.

He began his carrier working on RF noise suppression and signal integrity in RF sub-system assemblies at Picosecond Pulse Labs. Between 2007 and 2012, he was a principal microwave systems engineer working at FIRST RF Corporation in Boulder, CO, USA. While at FIRST RF he worked on a magnitude of specialized antenna systems ranging from 150MHz to 26.5GHz, with special focus surrounding unmanned aerial vehicle radar and communication systems.

Mr. Miers is currently pursuing a Ph.D. degree at the Department of Electrical and Information Technology, Lund University, Sweden. His main research interests include applications of characteristic modes in antenna design and development, low cost measurement hardware development, advanced mobile platform communication systems utilizing MIMO technology, and antenna design and implementation utilizing chassis coupled, traveling wave, and non-mechanical beam steering antennas.

Buon Kiong Lau (S'00–M'03–SM'07) received the B.E. degree (with honors) from the University of Western Australia, Perth, Australia, and the Ph.D. degree from the Curtin University of Technology, Perth, Australia, in 1998 and 2003, respectively, both in electrical engineering.

During 2000 to 2001, he was a Research Engineer with Ericsson Research, Kista, Sweden. From 2003 to 2004, he was a Guest Research Fellow at the Department of Signal Processing, Blekinge Institute of Technology, Sweden. Since 2004, he has been with the Department of Electrical and Information Technology, Lund University, where he is now an Associate Professor. He has been a Visiting Researcher with the Department of Applied Mathematics, Hong Kong Polytechnic University, China; the Laboratory for Information and Decision Systems, Massachusetts Institute of Technology, Cambridge, MA, USA; and the Takada Laboratory,

Tokyo Institute of Technology, Japan. His primary research interests are in various aspects of multiple antenna systems, particularly the interplay between antennas, propagation channels, and signal processing.

Dr. Lau is a Senior Associate Editor for the IEEE TRANSACTIONS ON ANTENNAS AND PROPAGATION, for which he was a Guest Editor of the 2012 Special Issue on MIMO Technology and is the Lead Guest Editor of the 2016

Special Issue on Theory and Applications of Characteristic Modes. He was the Lead Guest Editor of the 2013 Special Cluster on Terminal Antenna Systems for 4G and Beyond for the IEEE Antennas and Wireless Propagation Letters. From 2007 to 2010, he was a Co-Chair of Subworking Group 2.2 on "Compact Antenna Systems for Terminals" (CAST) within EU COST Action 2100. From 2011 to 2015, he has been a Swedish national delegate and the Chair of Subworking Group 1.1 on "Antenna System Aspects" within COST IC1004. From 2012-2015, he was the Regional Delegate of European Association on Antennas and Propagation (EurAAP) for Region 6 (Iceland, Norway, and Sweden). He is also a member of the Education Committee within the IEEE Antennas and Propagation Society (AP-S), where he served as the Coordinator for the annual IEEE AP-S Student Design Contest from 2013 to 2015.

In 2015, Dr. Lau received an award from the IEEE TRANSACTIONS ON ANTENNAS AND PROPAGATION for exceptional performance as an associate editor.